

Total cross section of the ${}^3\text{H}(p, n){}^3\text{He}$ reaction from threshold to 4.5 MeV

C. R. Brune*, K. I. Hahn†, R. W. Kavanagh, and P. R. Wrean‡

W. K. Kellogg Radiation Laboratory, 106-38

California Institute of Technology

Pasadena, CA 91125, USA

(October 16, 2018)

We report new measurements of the total cross section for the ${}^3\text{H}(p, n){}^3\text{He}$ reaction from threshold ($E_p = 1.02$ MeV) to $E_p = 4.5$ MeV. The experiment utilized specially prepared Ti- ${}^3\text{H}$ targets, and neutrons were detected using a 4π detector. A weak resonant structure due to an excited state in ${}^4\text{He}$ is observed which was not seen in previous cross section measurements. A new expression for the ${}^3\text{He}(n, p){}^3\text{H}$ thermonuclear reaction rate for temperatures below 10 GK is presented which will allow for more accurate calculations of the yields of light elements produced by big-bang nucleosynthesis.

PACS numbers: 25.10.+s; 26.35.+c; 28.20.-v; 98.80.Ft

I. INTRODUCTION

The ${}^3\text{H}(p, n){}^3\text{He}$ reaction and its inverse ${}^3\text{He}(n, p){}^3\text{H}$ are important in many subfields of physics. Due to its large cross section and other properties, this reaction is commonly used for two purposes in neutron physics: the ${}^3\text{H}(p, n){}^3\text{He}$ reaction is an important source of neutrons, and the ${}^3\text{He}(n, p){}^3\text{H}$ reaction is often used for detecting neutrons. This reaction also provides information about the excited levels of ${}^4\text{He}$, which are still not well understood [1,2]. The ${}^3\text{H}(p, n){}^3\text{He}$ reaction near threshold is strongly influenced by the first two excited levels of ${}^4\text{He}$, which lie 370 keV below and 430 keV above the ${}^3\text{H}(p, n){}^3\text{He}$ threshold, respectively [3]. The present experiment is primarily motivated by the role of this reaction in big-bang nucleosynthesis.

The standard big-bang model of the primordial universe is very successful in accounting for the observed relative abundances of the light elements ${}^2\text{H}$, ${}^3\text{He}$, ${}^4\text{He}$, and ${}^7\text{Li}$ [4–8]. The calculated abundances agree with observations only for baryon densities significantly lower than the critical density, in the range $0.01 \lesssim \Omega_B \lesssim 0.1$. The uncertainties in the abundance calculations arising from nuclear-data input have been studied in detail by Krauss and Romanelli [4] and Smith, Kawano, and Malaney [7]. The latter have identified 12 reactions which significantly affect light-element productions. Their assumed ${}^3\text{He}(n, p){}^3\text{H}$ reaction rate was found to have a significant impact on the calculated abundances of ${}^3\text{He}$ and ${}^7\text{Li}$. At the temperatures important for determining big-bang yields, the reaction rate is determined by the ${}^3\text{He}(n, p){}^3\text{H}$ cross section in the energy range $1 \lesssim E_{c.m.} \lesssim 250$ keV (see Sec. V below). In this energy range, the existing data are sparse, and not in good agreement.

Previous measurements of the ${}^3\text{H}(p, n){}^3\text{He}$ total cross section for $E_p \leq 4.5$ MeV have been reported by Vlasov *et al.* [9], Gibbons and Macklin [10], Perry *et al.* [11], and Macklin and Gibbons [12]. Unfortunately, two of the most important total cross section measurements [11,12] have been published only in conference proceedings or as a laboratory report.

The ${}^3\text{He}(n, p){}^3\text{H}$ cross section at thermal energies has been determined with high precision by the total cross section of Als-Nielsen and Dietrich [13]. Measurements at higher neutron energies have been reported by Coon [14], Batchelor, Aves, and Skyrme [15], Sayres, Jones, and Wu [16], Costello, Friesenhahn, and Lopez [17], and Borzakov *et al.* [18]. Ratios of the ${}^3\text{He}(n, p){}^3\text{H}$ cross section to the ${}^6\text{Li}(n, \alpha)$ and ${}^{10}\text{B}(n, \alpha)$ cross sections have been measured by Bergman and Shapiro [19] ($E_n \leq 30$ keV) and Bowman *et al.* [20] ($E_n \leq 25$ keV), respectively.

Recommended cross sections based on the available experimental data have been given by Costello [21], Liskien and Paulsen [22], Drogg [23], Drogg *et al.* [24], Bödy [25], Drogg and Schwerer [26], Hale, Dodder, and Young (ENDF/B-VI) [27], Smith, Kawano, and Malaney [7], and Drogg [28]. The ${}^3\text{H}(p, n){}^3\text{He}$ cross section at threshold is determined to better than 1% from the thermal ${}^3\text{He}(n, p){}^3\text{H}$ cross section [13], and the standard deviation in the evaluated cross section is estimated to be 4% or less for $2 \leq E_p \leq 16$ MeV [26]. Between threshold and 2 MeV, most of the experiments

*Present address: University of North Carolina at Chapel Hill, Chapel Hill, NC 27599-3255, USA and Triangle Universities Nuclear Laboratory, Durham, NC 27708-0308, USA

†Present address: Department of Science Education, Ewha Women's University, Seoul 120-750, Korea

‡Present address: TRIUMF, Vancouver, BC, Canada V6T 2A3.

have errors of 10% or greater. The recent and accurate (2-3% quoted uncertainty) measurements of the ${}^3\text{He}(n,p){}^3\text{H}$ cross section for $E_n \leq 137$ keV [18] disagree with the energy dependence found by Ref. [12] by about 25%, and also disagree with the ENDF/B-VI evaluation by up to 15%. The energy range for big-bang nucleosynthesis lies between threshold and 2 MeV; it is the large uncertainty within this energy range which motivates the present work.

In this paper, we report new measurements of the ${}^3\text{H}(p,n){}^3\text{He}$ total cross section, from threshold to $E_p = 4.5$ MeV. A new thermonuclear reaction rate is calculated which is valid for temperatures less than 10 GK.

II. EXPERIMENTAL APPARATUS AND PROCEDURES

A. Beam

The proton, deuteron, and ${}^4\text{He}^+$ beams used in this experiment were supplied by the Caltech 3-MV Pelletron Tandem Accelerator. The beam energy was defined by a 90° analyzer magnet and NMR magnetometer. The energy calibration ($\pm 0.1\%$) was established using the resonances at 483.91 ± 0.10 -keV [29] in ${}^{19}\text{F}(p, \alpha\gamma)$, 991.86 ± 0.03 -keV [30] in ${}^{27}\text{Al}(p, \gamma)$, 606.0 ± 0.5 -keV [31] in ${}^{11}\text{B}(\alpha, n)$, and 1530.03 ± 0.15 -keV [32] in ${}^{24}\text{Mg}(\alpha, \gamma)$. A collimator limited the beam to an area of ≈ 1 cm² on the targets; the beam was rastered over this area in order to produce a uniform intensity distribution. Beam currents for the ${}^3\text{H}(p,n){}^3\text{He}$ measurements varied between 7 and 100 nA, depending on the desired counting rate. The number of incident particles was determined by beam-current integration, to a precision of $\pm 1\%$.

B. Targets

The preparation, characterization, and use of the Ti- ${}^3\text{H}$ targets have been described previously [33–35]. Briefly, Ti was evaporated onto 31.7-mm-diameter, 0.81-mm-thickness Cu or Ta substrates; the substrates were then heated in an atmosphere of ${}^3\text{H}_2$ gas to induce the formation of Ti- ${}^3\text{H}$. The substrates were maintained in high vacuum during the time between Ti evaporation and tritide formation, minimizing contamination and maximizing the attainable ${}^3\text{H}:\text{Ti}$ ratio.

The ${}^3\text{H}$ and Ti areal densities were determined in a scattering chamber using the ${}^3\text{H}(d, \alpha)$ and $\text{Ti}(\alpha, \alpha)$ reactions, respectively. The total cross section and center-of-mass Legendre coefficients for ${}^3\text{H}(d, \alpha)$ reaction, needed for the absolute ${}^3\text{H}$ areal-density determination, were taken from the evaluation of Drog and Schwerer [26]; the uncertainty in the cross section is estimated to be 1.5% for $E_d < 400$ keV, increasing to 4% for higher energies. The absolute uncertainty in the areal density determinations is estimated to be $\pm 4\%$.

Two targets were utilized for the ${}^3\text{H}(p,n){}^3\text{He}$ measurements. One target consisted of 5.52×10^{17} and 2.96×10^{17} atoms/cm² of ${}^3\text{H}$ and Ti, respectively, on a Cu backing. This target is referred to as “target 1” in Ref. [35]; $\text{Ti}(\alpha, \alpha)$ and ${}^3\text{H}(d, \alpha)$ spectra obtained with this target are shown in Figs. 4 and 6 of Ref. [33]. The use of this target for ${}^3\text{H}(p,n){}^3\text{He}$ measurements is limited to energies below the ${}^{65}\text{Cu}(p,n)$ threshold at $E_p = 2.17$ MeV. To facilitate measurements at higher energies an additional target was fabricated on a Ta backing with 8.30×10^{17} and 9.5×10^{17} atoms/cm² of ${}^3\text{H}$ and Ti, respectively. The ${}^3\text{H}(d, \alpha)$ excitation function obtained with this target is shown in Fig. 7 of Ref. [33]. The ${}^3\text{H}(p,n){}^3\text{He}$ measurements reported here were performed before these targets were used for any other experiments.

Two additional targets were used to investigate backgrounds from targets containing no ${}^3\text{H}$. One target consisted of 4.36×10^{17} and 2.98×10^{17} atoms/cm² of ${}^2\text{H}$ and Ti, respectively, and was produced on a Cu backing using the same equipment as for the ${}^3\text{H}$ targets. The other target consisted of 1.0×10^{18} Ti atoms/cm² evaporated on a Ta backing, and was not hydrided.

C. Neutron detection

Neutrons were detected in a 4π detector consisting of up to 12 ${}^3\text{He}$ -filled proportional counters embedded in a polyethylene moderator surrounding the target chamber. The efficiency is slowly varying in the region $0.0005 < E_n < 2$ MeV, such that it can be approximated by a constant within $\pm 10\%$. However, the efficiency drops dramatically outside of this range, by about a factor of two for 1-eV or 5-MeV neutrons. For a known distribution of neutron energies and emission angles, the efficiency can be more accurately determined from Monte Carlo simulations. For this purpose we utilize the computer code MCNP [36], which simulates the transport and detection of neutrons, given

the materials and geometry of our target holders and detector. Additional information concerning the detector, the Monte Carlo simulations, and experimental validation of the simulations is given in Refs. [37,38].

One set of ${}^3\text{H}(p, n){}^3\text{He}$ measurements was taken using 11 detection tubes in the moderator, with one additional tube present but not used. The other set of measurements was taken using 6 tubes in the moderator. The angular distributions of neutrons emitted from the ${}^3\text{H}(p, n){}^3\text{He}$ reaction, required to determine the (correlated) distributions of neutron energies and emission angles in the Monte Carlo simulations, were taken from Ref. [26]. In order to investigate the sensitivity of the simulations to the assumed angular distributions, we also performed simulations assuming that the reaction is isotropic in the center-of-mass system. The resulting efficiencies differed by at most 2% for $E_p \leq 4.5$ MeV, indicating an uncertainty of $< 1\%$ from the assumed angular distributions. The simulated efficiencies for the 6-tube configuration were renormalized by 1.02, so that the ratio of measured to simulated efficiency for a ${}^{252}\text{Cf}$ neutron source was the same for both sets of measurements. This procedure standardizes the measurements to the configuration for which the efficiency of the detector has been extensively tested [37]. The results of the simulations for the two detector configurations are shown in Fig. 1. Also shown as solid lines are empirical fits used in subsequent analysis. We estimate the systematic uncertainty in the neutron detection efficiency to be $\pm 3\%$.

D. Yield measurements

The neutron yield with the Cu-backed ${}^3\text{H}$ target perpendicular to the beam was measured with the 11-tube detector configuration for $1.016 \leq E_p \leq 2.15$ MeV, i.e., from just below the ${}^3\text{H}(p, n){}^3\text{He}$ threshold to just below the ${}^{65}\text{Cu}(p, n)$ threshold.

The yield with the Ta-backed ${}^3\text{H}$ target at 45° with respect to the beam was measured with 6 tubes from just below threshold to $E_p = 4.5$ MeV. The measured yields are displayed in the upper panel of Fig. 2. The yields were corrected for dead time in the detector ($\leq 2\%$ for all measurements). Repeated measurements at a standard energy of $E_p = 1.3$ MeV indicated that the target thickness deteriorated by less than 1% over the course of the measurements. The stability of the detection system was monitored throughout the experiment by measuring the efficiency for a ${}^{252}\text{Cf}$ neutron source.

Beam-off backgrounds were completely negligible for this experiment. It is however important to consider possible backgrounds from other neutron-producing reactions which may take place in the target. Of particular concern here are the ${}^{49}\text{Ti}(p, n)$ and ${}^{50}\text{Ti}(p, n)$ reactions which have thresholds at proton energies of 1.41 and 3.05 MeV, respectively. In order to test for possible backgrounds, measurements were made using targets without ${}^3\text{H}$ (these targets are described in Subsec. II B). The Ti- ${}^2\text{H}$ target was measured with the same target angle and neutron detector configuration as the Cu-backed ${}^3\text{H}$ target; the Ti target on Ta backing was measured under the same conditions as the Ta-backed ${}^3\text{H}$ target. The results of these measurements are shown on the lower panel of Fig. 2.

III. DATA ANALYSIS AND RESULTS

The magnitude and energy dependence of the beam-dependent background observed from targets containing no ${}^3\text{H}$ are consistent with the known ${}^{48}\text{Ti}(p, n)$ [39] and ${}^{49}\text{Ti}(p, n)$ [40] cross sections. Using the known Ti areal density, the background present in the measurements using the Cu-backed ${}^3\text{H}$ target is estimated to be at most 0.2%, and was therefore neglected. For the Ta-backed ${}^3\text{H}$ target, the background is estimated to be $< 1\%$ for $E \leq 3.2$ MeV. For $E_p \geq 2.0$ MeV the yields measured from this target were corrected for background, using the solid curve shown in Fig. 2, scaled by the ratio of Ti areal densities. This correction was at most 7%, at $E_p = 4.5$ MeV. An error of $\pm 30\%$ was assumed for the subtracted yield.

The background-corrected yield of neutrons detected per incident particle Y_n , for a mono-energetic beam of energy E_p , is given by

$$Y_n = (nt) \sigma(E_p) \varepsilon(E_p), \quad (1)$$

where (nt) is the areal number density of target atoms, σ is the ${}^3\text{H}(p, n){}^3\text{He}$ cross section, and ε is the neutron-detection efficiency. For a target of significant thickness, the beam loses energy as it passes through the target, and the yield is then given by

$$Y_n = \int_{E_t}^{E_p} \sigma(E'_p) \varepsilon(E'_p) \left[\frac{dE}{dX}(E'_p) \right]^{-1} dE'_p, \quad (2)$$

in which $E_t = E_p - \Delta E$, where E_p is the incident proton energy and ΔE is the energy loss in the target. The energy loss of protons in the target per ${}^3\text{H}$ atom per unit area is given by

$$\frac{dE}{dX} = \left(\frac{dE}{dX}\right)_{\text{H}} + \frac{1}{r} \left(\frac{dE}{dX}\right)_{\text{Ti}}, \quad (3)$$

where $(\frac{dE}{dX})_{\text{H}}$ and $(\frac{dE}{dX})_{\text{Ti}}$ are the stopping powers for protons in H and Ti [41], and r is the ${}^3\text{H}:\text{Ti}$ ratio which is assumed to be independent of depth in the target. The energy loss for 2-MeV α particles in the Ti- ${}^3\text{H}$ computed by this method has been verified experimentally for these targets [33].

Some indication of the consistency of the beam-energy calibration and the quality of the targets is provided by the behavior of the neutron yield near the threshold. For a target sufficiently thick to integrate the cross section down to the threshold energy E_0 , the detected neutron yield varies as $Y_n \propto (E_p - E_0)^{3/2}$, provided the neutron production cross section varies as $(E_p - E_0)^{1/2}$ (i.e., assuming s -wave neutrons and no narrow resonance). This simple analysis also assumes that the energy dependences of the stopping power and detection efficiency are negligible. A linear fit to $Y_n^{2/3}$ should thus intersect the E_p axis at the threshold energy. Plots of $Y_n^{2/3}$ versus E_p for the two targets are shown in Fig. 3. The yield from the Cu-backed target departs from a linear dependence more quickly than the Ta-backed target due to its smaller thickness. Linear fits are also shown which included points within ≈ 4 keV of threshold for the Cu-backed target and within ≈ 10 keV of threshold for the Ta-backed target. Note that 1-MeV protons lose 4.8 keV and 22 keV in the Ti- ${}^3\text{H}$ layer for the Cu-backed and Ta-backed targets, respectively. Both fits give a threshold energy of 1.0188 MeV, which is in excellent agreement with the known value 1.01906 MeV¹.

Cross sections were extracted from the measured yields using Eqs. (7)-(9) of Ref. [43] to correct for the energy loss effects described by Eq. (2). This procedure requires that the energy dependence of the cross section be known in advance. For this purpose we assumed the ENDF/B-VI evaluation, converted to ${}^3\text{H}(p, n){}^3\text{He}$ using detailed balance. The assumed energy dependence is only important near threshold where the cross section changes significantly as the beam loses energy in the target. For $E_p \geq 1.1$ MeV this procedure differs negligibly from using Eq. (1) with E_p replaced by $E_p - \Delta E/2$, due to the thin targets used in the experiment. The data were also analyzed assuming $\sigma \propto (E_p - E_0)^{1/2}$, which for all incident energies changed the resulting cross sections by an amount negligible compared to other uncertainties. One important source of error near the threshold is the energy of the incident proton beam. Given the good agreement obtained with the known threshold energy already described, we have allowed for an uncertainty of ± 0.5 keV in the incident energy. We have also allowed for $\pm 10\%$ uncertainty in the proton energy loss. We do not present the data where $E_p \leq E_0 + \Delta E$ due to the large errors from uncertainties in the incident energy and energy loss. The error bars on the data points include uncertainties from counting statistics, incident energy, energy loss, and background subtraction. Additional systematic errors in the data are summarized in Table I.

The absolute cross sections determined from the Ta-backed target are $\approx 2\%$ higher than from the Cu-backed target. The data sets were renormalized to a scale corresponding to the arithmetic mean of the two determinations. The final results for the total cross section are shown in Fig. 4. The behavior of the cross section near the threshold is more easily seen by converting the data to ${}^3\text{He}(n, p){}^3\text{H}$ cross sections using detailed balance and multiplying by $E_n^{1/2}$, as shown for the near-threshold data in Fig. 5. The rather large systematic errors associated with the lowest-energy data points shown in Fig. 5 arise from the uncertainty in proton energy, as the detailed-balance conversion is very sensitive to the proton energy when the proton energy is near threshold.

IV. DISCUSSION

A. Comparison to previous measurements

We will not attempt to compare our new results to all of the data available with $E_p \leq 4.5$ MeV. The reader is referred to the evaluations [7,21,22,24-27], and in particular Ref. [23] for a critique of the previous measurements. Some additional information related to previous experiments is also supplied in the Appendix. In Fig. 4 our cross-section data are compared to two recent evaluations [27,28]. It is seen that both evaluations are in excellent agreement with the present data, with a maximum deviation of $\approx 5\%$ near $E_p = 2.7$ MeV, but within our estimated systematic error.

In Figs. 6 and 7 the data are compared to some of the previous data in the energy range appropriate for big-bang nucleosynthesis. The data are in general agreement with most of the other older measurements which had considerably

¹All thresholds and detailed balance conversions in this paper are computed using relativistic kinematics with nuclear masses; Q -values and atomic masses are taken from Audi and Wapstra [42]. The uncertainty in the Q value (≈ 0.002 keV) is sufficiently small to be a negligible consideration in the detailed-balance conversions.

larger errors. The data agree well with results of Borzakov *et al.* [18], except for their higher-energy data points. Our results are not in agreement with the data from Macklin and Gibbons [12], especially for their higher energies. It should be noted however that the scale of their data is not absolute, so the discrepancy is in the energy dependence.

B. Excited levels of ${}^4\text{He}$

The present data show the near-threshold energy dependence of the cross section much more clearly than previous measurements. In particular, it is clear from inspection of Fig. 5 that the cross section deviates from the $1/v$ energy dependence expected for non-resonant s -wave neutron-induced reactions (a $1/v$ dependence would yield a horizontal line when multiplied by $E_n^{1/2}$). The observed energy dependence results primarily from the first three excited levels of ${}^4\text{He}$ located [3] at $E_x = 20.21$ MeV ($J^\pi = 0^+$), 21.01 MeV ($J^\pi = 0^-$), and 21.84 MeV ($J^\pi = 2^-$); note that the location of the ${}^3\text{He} + n$ threshold is at $E_x = 20.58$ MeV. As discussed by Borzakov *et al.* [18] and references therein, the cross section very near threshold is dominated by the subthreshold 0^+ s -wave resonance.

At higher energies, the effects of the other levels become important. The present data as shown in Fig. 4 indicate a definite change in curvature near $E_p = 1.6$ MeV. In previous experiments this feature was masked by the larger errors and/or coarser energy steps. Interestingly, this feature is predicted very well by the ENDF/B-VI evaluation [27] (see Fig. 4 of the present work). The ENDF/B-VI evaluation for ${}^3\text{He}(n,p){}^3\text{H}$ is generated from an R -matrix analysis [44] which is essentially the same as that described in Ref. [3]. This charge-independent R -matrix analysis includes cross-section and polarization data for $n - {}^3\text{He}$, $p - {}^3\text{H}$, and ${}^2\text{H} - {}^2\text{H}$ scattering and reactions; and $p - {}^3\text{He}$ and $n - {}^3\text{H}$ scattering. The curvature near $E_p = 1.6$ MeV results from the 0^- second excited state of ${}^4\text{He}$. A recent measurement of the longitudinal polarization-transfer coefficient near $E_p = 1.6$ MeV [45] has provided striking evidence for this level. These authors conclude that at the peak of the 0^- resonance near $E_p = 1.6$ MeV, the reaction is dominated by 0^+ and 0^- amplitudes which are approximately equal in strength. At higher energies additional levels become important, especially the 2^- state at $E_x = 21.84$ MeV which gives rise to the broad peak in the ${}^3\text{H}(p,n){}^3\text{He}$ cross section near $E_p = 3.0$ MeV. The data presented here will help to establish more accurately the properties of these excited levels of ${}^4\text{He}$.

V. THERMONUCLEAR REACTION RATE

The two-body thermonuclear reaction rate $N_A\langle\sigma v\rangle$ is calculated from the cross section σ using

$$N_A\langle\sigma v\rangle = \left(\frac{8}{\pi\mu}\right)^{1/2} \frac{N_A}{(kT)^{3/2}} \int_0^\infty E \sigma(E) \exp\left(-\frac{E}{kT}\right) dE, \quad (4)$$

where N_A is Avogadro's number, μ is the reduced mass in the entrance channel, k is Boltzmann's constant, T is temperature, and E is the center-of-mass energy.

Several tests were carried out to determine the effect of the ${}^3\text{He}(n,p){}^3\text{H}$ reaction rate on the primordial nucleosynthesis yields of the light elements ${}^2\text{H}$, ${}^3\text{He}$, ${}^4\text{He}$, and ${}^7\text{Li}$. Standard big-bang nucleosynthesis calculations were performed using the computer code described in Ref. [46]. The calculation assumes that the baryon density is homogeneous, and that there are three neutrino species. We find that $\pm 10\%$ changes in the ${}^3\text{He}(n,p){}^3\text{H}$ reaction rate lead to changes of order 10% in the ${}^3\text{He}$ and ${}^7\text{Li}$ abundances, changes of order 1% in the ${}^2\text{H}$ abundance, and no change in the ${}^4\text{He}$ abundance. The magnitude and direction of the changes are dependent upon the value of the baryon-to-photon ratio η . These findings are in agreement with the results of Smith, Kawano, and Malaney [7]. In order to determine the energy range where the cross section is important, we have also varied the reaction rate at different temperatures. The final abundances of the light elements are found to depend on the reaction rate in the temperature range $20 \leq kT \leq 60$ keV, or equivalently $0.2 \leq T_9 \leq 0.7$, where T_9 is the temperature in GK. Changes in the reaction rate outside of this temperature range do not affect the final abundances (at least for baryon-to-photon ratios in the generally accepted range $1 \leq 10^{10}\eta \leq 10$). This temperature range corresponds approximately to the center-of-mass energy range $1 \lesssim E \lesssim 250$ keV in the $n - {}^3\text{He}$ system, which is almost entirely covered by the present experimental results.

For the calculation of the ${}^3\text{He}(n,p){}^3\text{H}$ thermonuclear reaction rate, we assumed the cross section given by ENDF/B-VI evaluation [27]. This evaluation reproduces the well-known thermal cross section [13], and as can be seen in Fig. 5 lies $\approx 3\%$ higher than the present experimental results for $E_n \leq 1$ MeV. This deviation is considerably smaller than our estimated systematic uncertainty in the experimental data. Using this parameterization, the reaction rate $N_A\langle\sigma v\rangle$ was then calculated by numerically integrating Eq. (4). Our numerically integrated reaction rate is given within 1.5% for $T_9 \leq 10$ by the following expression (plotted in Fig. 8):

$$N_A \langle \sigma v \rangle = 7.05 \times 10^8 (1 - 0.648T_9^{1/2} + 0.426T_9 - 0.068T_9^{3/2}). \quad (5)$$

We estimate the uncertainty in this reaction rate to be 5% in the temperature range important for big-bang nucleosynthesis calculations. In the important temperature range, the new rate is $\approx 5\%$ lower than that given by Smith, Kawano, and Malaney [7], and 15-25% lower than that given by Caughlan and Fowler [47].

VI. CONCLUSIONS

We have measured the ${}^3\text{H}(p, n){}^3\text{He}$ cross section for $1.02 \leq E_p \leq 4.50$ MeV, with a systematic uncertainty estimated to be 5%. These measurements are considerably more accurate than the previously available data over most of the energy range. The data near $E_p = 1.6$ MeV show the subtle effects of the 0^- second excited state of ${}^4\text{He}$ which were not apparent in previous ${}^3\text{H}(p, n){}^3\text{He}$ cross section measurements. In the future it may also be possible to compare the present data to calculations which utilize realistic nuclear forces. Calculations of this type have recently been performed for $n - {}^3\text{H}$ and $p - {}^3\text{He}$ scattering at zero energy [53].

A new thermonuclear reaction rate for ${}^3\text{He}(n, p){}^3\text{H}$ has been calculated from the ENDF/B-VI evaluation [27] which agrees very well with the present data and the accurately known thermal cross section [13]. This rate will allow for more accurate calculations of the big-bang yields of ${}^3\text{He}$ and ${}^7\text{Li}$. These calculations can then in turn be used to test the consistency of the big-bang model as well as to determine the baryon-to-photon ratio.

ACKNOWLEDGMENTS

We thank G. M. Hale and M. Drogg for providing useful information concerning the ${}^3\text{H}(p, n){}^3\text{He}$ reaction. This work was supported in part by the National Science Foundation, Grant No. PHY91-15574. The final stages of this work were completed at the Triangle Universities Nuclear Laboratory, supported in part by the U. S. Department of Energy, Grant No. DE-FG02-97ER41041.

APPENDIX: PREVIOUS DATA

As a result of our literature search for previous data, several important aspects related to previous measurements have become apparent which we would like to make more widely known. This information should be particularly useful to future evaluators of the ${}^3\text{H}(p, n){}^3\text{He}$ or ${}^3\text{He}(n, p){}^3\text{H}$ cross sections. These aspects have not always been noted in the past. The work of Drogg [23] provided the basis for much of this discussion.

(1) In addition to the data cited in the Introduction, the ${}^3\text{H}(p, n){}^3\text{He}$ total cross section can be inferred from other types of measurements. For example, absolute 0° differential cross section measurements can be combined with angular distribution data to give total cross sections. Data of this type are given in Refs. [22–24,26], and references therein. The total cross section for ${}^3\text{He}(n, p){}^3\text{H}$ can also be found by subtracting the elastic neutron cross section from the total neutron cross section (see Seagrave, Cranberg, and Simmons [48] and Alfimenkov *et al.* [49]). However, since the (n, p) cross section is a small fraction of the total cross section (for $E_n \gtrsim 50$ keV), this subtraction can be subject to rather large uncertainties.

(2) Some ${}^3\text{He}(n, p){}^3\text{H}$ measurements are dependent on the absolute $n - {}^3\text{He}$ total cross section. There are significant discrepancies in the existing $n - {}^3\text{He}$ total cross section measurements (see Ref. [23] for details). The $n - {}^3\text{He}$ total cross section affects the data from Refs. [48,49] mentioned in the previous paragraph and also from Refs. [16,17] which measured the ratio of the ${}^3\text{He}(n, p){}^3\text{H}$ cross section to the $n - {}^3\text{He}$ total cross section.

(3) Some reported measurements have been superseded by or included in subsequent data sets, and should be considered accordingly. The data of Jarvis *et al.* [50] are renormalized and included with additional data in Ref. [51]. The data of Ref. [51] are then apparently included in revised form in Ref. [11] (see Ref. [23]). Also, the data of Macklin and Gibbons [52] have been renormalized in their later work [10].

[1] H. M. Hofmann and G. M. Hale, Nucl. Phys. **A613**, 69 (1997).

- [2] A. Csóto and G. M. Hale, Phys. Rev. C **55**, 2366 (1997).
- [3] D. R. Tilley, H. R. Weller, and G. M. Hale, Nucl. Phys. **A541**, 1 (1992).
- [4] L. M. Krauss and P. Romanelli, Astrophys. J. **358**, 47 (1990).
- [5] S. P. Riley and J. M. Irvine, J. Phys. G **17**, 35 (1991).
- [6] T. P. Walker, G. Steigman, D. N. Schramm, K. A. Olive, and H.-S. Kang, Astrophys. J. **376**, 51 (1991).
- [7] M. S. Smith, L. H. Kawano, and R. A. Malaney, Astrophys. J., Suppl. Ser. **85**, 219 (1993).
- [8] C. J. Copi, D. N. Schramm, and M. S. Turner, Science **267**, 192 (1995).
- [9] N. A. Vlasov, S. P. Kalinin, A. A. Ogloblin, L. N. Samoilov, V. A. Sidorov, and V. I. Chuev, Sov. Phys. – JTEP **1**, 500 (1955).
- [10] J. H. Gibbons and R. L. Macklin, Phys. Rev. **114**, 571 (1959).
- [11] J. E. Perry, E. Haddad, R. I. Henkel, G. A. Jarvis, and R. K. Smith, quoted by J. D. Seagrave, in *Nuclear Forces and the Few-Nucleon Problem*, proceedings of the International Conference, London, edited by T. C. Griffith and E. A. Power (Pergamon, Oxford, 1960), Volume II, p. 583. The data are given in numerical form in Ref. [22].
- [12] R. L. Macklin and J. H. Gibbons, in *Nuclear Structure Study with Neutrons*, proceedings of the International Conference on the Study of Nuclear Structure with Neutrons, Antwerp, edited by M. Nève de Mévergnies, P. Van Assche, and J. Vervier (North-Holland, Amsterdam, 1966), p. 498; Oak Ridge National Laboratory Report No. ORNL-P-1375, 1965. The data are given in numerical form in Ref. [22].
- [13] J. Als-Nielsen and O. Dietrich, Phys. Rev. **133**, B925 (1964).
- [14] J. H. Coon, Phys. Rev. **80**, 488 (1950).
- [15] R. Batchelor, R. Aves, and T. H. R. Skyrme, Rev. Sci. Instrum. **26**, 1037 (1955).
- [16] A. R. Sayres, K. W. Jones, and C. S. Wu, Phys. Rev. **122**, 1853 (1961).
- [17] D. G. Costello, S. J. Friesenhahn, and W. M. Lopez, Nucl. Sci. Eng. **39**, 409 (1970).
- [18] S. B. Borzakov, H. Malecki, L. B. Pikel’ner, M. Stempinski, and É. I. Sharapov, Yad. Fiz. **35**, 532 (1982).
- [19] A. A. Bergman and F. L. Shapiro, Sov. Phys. – JTEP **13**, 895 (1961).
- [20] C. D. Bowman, J. W. Behrens, R. Gwin, and J. H. Todd, in *Nuclear Cross Sections for Technology*, proceedings of the International Conference, Knoxville, Tennessee, edited by J. L. Fowler, C. H. Johnson, and C. D. Bowman (U. S. Dept. of Commerce, 1980), p. 97.
- [21] D. G. Costello, in *Neutron Standards and Flux Normalization*, proceedings of a symposium, Argonne, Illinois, coordinated by A. B. Smith (U. S. Atomic Energy Commission, 1971), p. 74.
- [22] H. Liskien and A. Paulsen, Nucl. Data Tables **11**, 569 (1973).
- [23] M. Drosog, Los Alamos National Laboratory Report No. LA-8215-MS, 1980.
- [24] M. Drosog, G. Haouat, W. Stoeffel, and D. M. Drake, Los Alamos National Laboratory Report No. LA-10444-MS, 1985.
- [25] Z. Bödy, in *Handbook on Nuclear Activation Data* (International Atomic Energy Agency, Vienna, 1987), p. 29.
- [26] M. Drosog and O. Schwerer, in *Handbook on Nuclear Activation Data* (International Atomic Energy Agency, Vienna, 1987), p. 83.
- [27] G. Hale, D. Dodder, and P. Young, “ENDF/B-VI Data File for ^3He ,” National Nuclear Data Center, Brookhaven National Laboratory, Upton, New York, 1991 (unpublished).
- [28] M. Drosog, computer code DROSG-96, International Atomic Energy Agency, Nuclear Data Section, 1996.
- [29] F. Ajzenberg-Selove, Nucl. Phys. **A475**, 1 (1987).
- [30] P. M. Endt, Nucl. Phys. **A521**, 1 (1990).
- [31] T. R. Wang, R. B. Vogelaar, and R. W. Kavanagh, Phys. Rev. C **43**, 883 (1991); **44**, 1226(E) (1991).
- [32] J. W. Maas, A. J. C. D. Holvast, A. Baghus, H. J. M. Aarts, and P. M. Endt, Nucl. Phys. **A301**, 213 (1978).
- [33] C. R. Brune and R. W. Kavanagh, Nucl. Instrum. Methods **A343**, 415 (1994).
- [34] C. R. Brune, Ph.D. thesis, California Institute of Technology, 1994.
- [35] C. R. Brune, R. W. Kavanagh, and C. Rolfs, Phys. Rev. C **50**, 2205 (1994).
- [36] J. F. Breisemeister, computer code MCNP, Version 4A, Los Alamos National Laboratory Report No. LA-12625-M, 1993.
- [37] P. R. Wrean, Ph.D. thesis, California Institute of Technology, 1998.
- [38] P. R. Wrean and R. W. Kavanagh, to be published.
- [39] S. R. Kennett, M. R. Anderson, Z. E. Switkowski, and D. G. Sargood, Nucl. Phys. **A344**, 351 (1980).
- [40] S. R. Kennett, M. R. Anderson, L. W. Mitchell, Z. E. Switkowski, and D. G. Sargood, Nucl. Phys. **A346**, 523 (1980).
- [41] J. F. Ziegler, *The Stopping and Ranges of Ions In Matter* (Pergamon, New York, 1977) Vols. 3 and 4.
- [42] G. Audi and A. H. Wapstra, Nucl. Phys. **A595**, 409 (1995).
- [43] P. R. Wrean, C. R. Brune, and R. W. Kavanagh, Phys. Rev. C **49**, 1205 (1994).
- [44] G. M. Hale (private communication).
- [45] J. R. Walston, C. D. Keith, C. R. Gould, D. G. Haase, B. W. Raichle, M. L. Seely, W. Tornow, W. S. Wilburn, G. W. Hoffmann, and S. I. Penttilä, Phys. Rev. C **58**, 1314 (1998).
- [46] L. H. Kawano, computer code NUC123 (1992); Caltech Kellogg Radiation Lab OAP-714, preprint; FERMILAB-PUB-92/04-A, preprint.
- [47] G. R. Caughlan and W. A. Fowler, At. Data Nucl. Data Tables **40**, 283 (1988).
- [48] J. D. Seagrave, L. Cranberg, and J. E. Simmons, Phys. Rev. **119**, 1981 (1960).

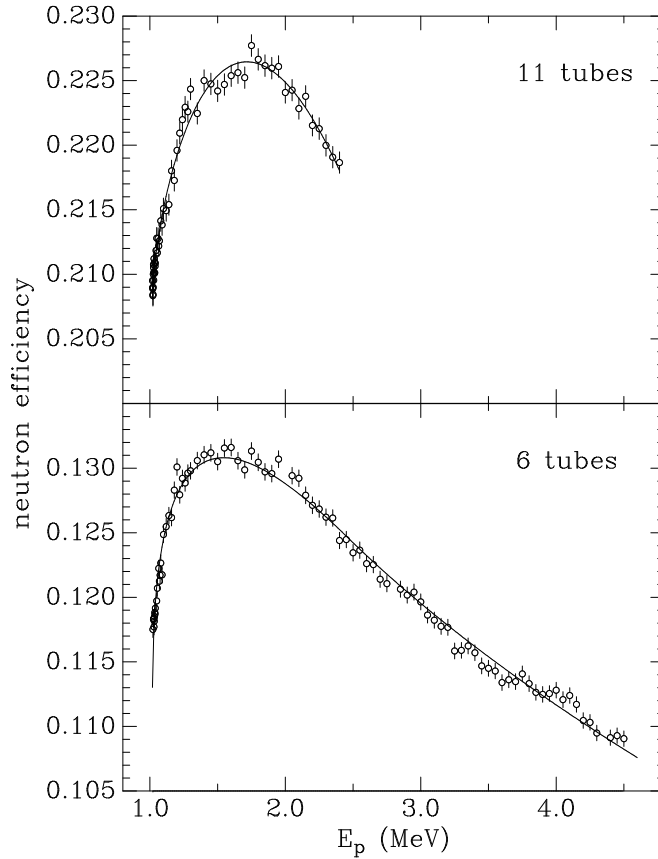


FIG. 1. The neutron efficiency as a function of proton energy for the 11-tube configuration (top panel) and the 6-tube configuration (bottom panel). The Monte Carlo calculations with statistical errors are shown as circles, and the solid curves are empirical fits used in subsequent calculations. Note the break in vertical scale between the two panels.

- [49] V. P. Alfimenkov, S. B. Borzakov, Vo Van Tkhuan, A. M. Govorov, L. Lason, L. B. Pikel'ner, and É. A. Sharapov, *Yad. Fiz.* **33**, 891 (1981).
- [50] G. A. Jarvis, A. Hemmendinger, H. V. Argo, and R. F. Taschek, *Phys. Rev.* **79**, 929 (1950).
- [51] N. Jarmie and J. D. Seagrave, Los Alamos National Laboratory Report No. LA-8215-MS, 1980.
- [52] R. L. Macklin and J. H. Gibbons, *Phys. Rev.* **109**, 105 (1958).
- [53] M. Viviani, S. Rosati, and A. Kievsky, *Phys. Rev. Lett.* **81**, 1580 (1998).

TABLE I. Systematic errors in the absolute cross-section data not included in the plotted error bars. The total is computed by adding the individual errors in quadrature.

Source of Error	Error (%)
^3H areal density	4
neutron detection efficiency	3
current integration	1
total	5

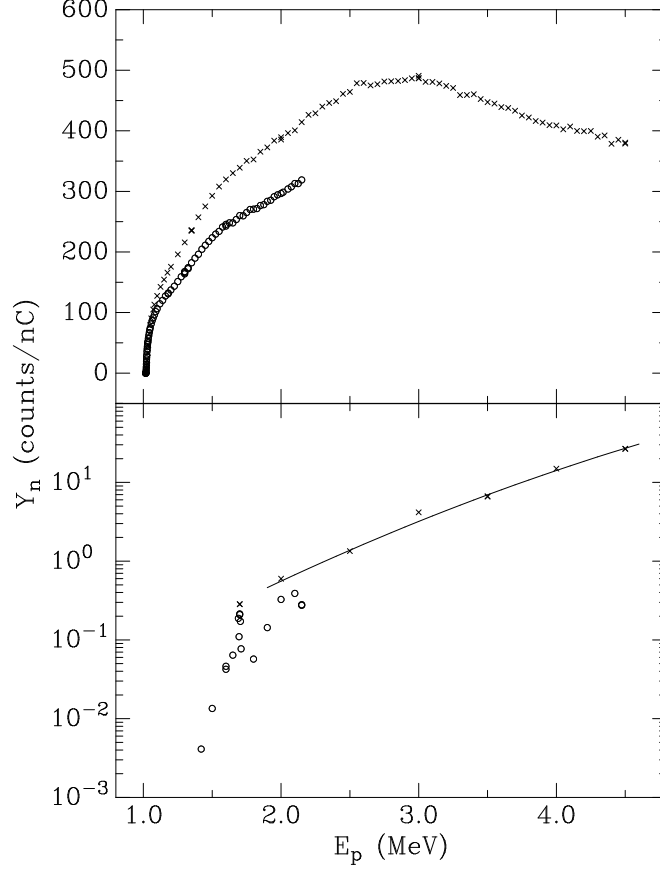


FIG. 2. Yields Y_n of detected neutrons for various targets. Upper panel: For the Cu-backed (\circ) and Ta-backed (\times) ^3H targets. Lower panel: For the Cu-backed (\circ) and Ta-backed (\times) targets used for background measurements. The statistical errors are smaller than the size of the data points. The solid curve is an empirical fit used for background subtraction.

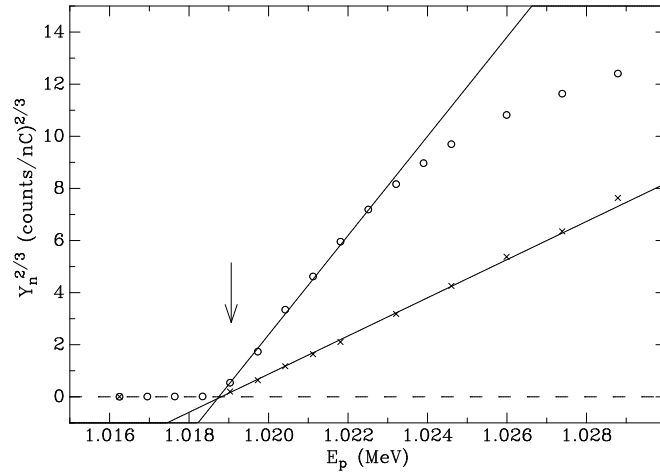


FIG. 3. The near-threshold yield of detected neutrons (raised to the $2/3$ power) for the Cu-backed target (\circ) and the Ta-backed target (\times). The statistical errors are smaller than the size of the data points. The solid lines are linear fits described in the text. The arrow indicates the known threshold energy. The different slopes for the two targets are caused by differences in neutron-detection efficiency and the $^3\text{H}:\text{Ti}$ ratio.

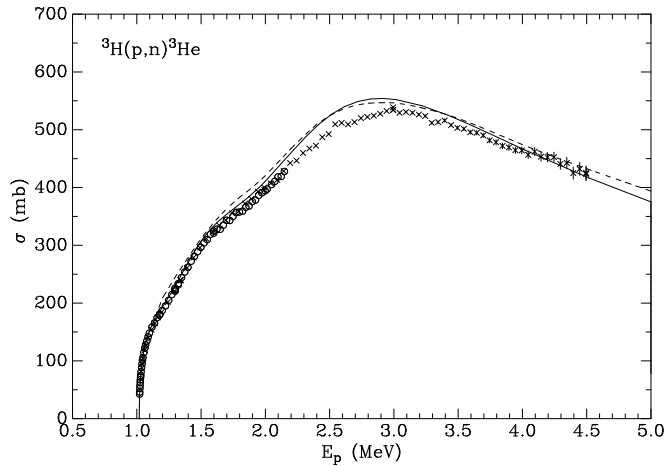


FIG. 4. The present results for the ${}^3\text{H}(p,n){}^3\text{He}$ total cross section, for the Cu-backed target (\circ) and Ta-backed target (\times). When not visible, the errors are smaller than the size of the data points (the additional systematic uncertainty of 5% described in Table I is not included). The solid curve is ENDF/B-VI evaluation [27] and the dashed curve is the evaluation from the DROSG-96 computer code [28].

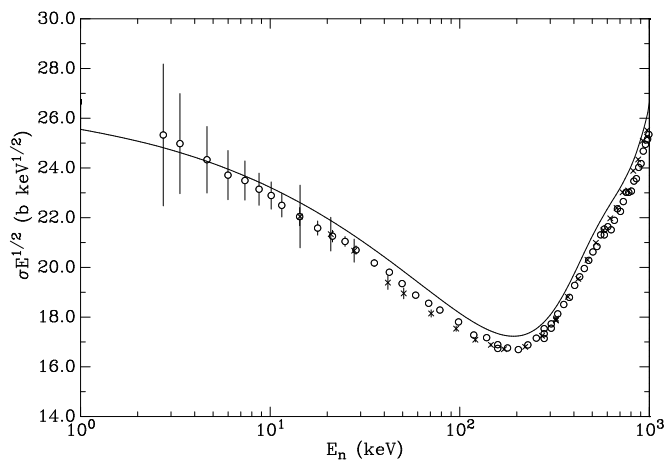


FIG. 5. The results, converted to ${}^3\text{He}(n,p){}^3\text{H}$, and multiplied by $E_n^{1/2}$. The plot symbols have the same meaning as in Fig. 4. When not visible, the errors are smaller than the size of the data points (the systematic uncertainty of 5% described in Table I is not included). The solid curve is the ENDF/B-VI evaluation [27].

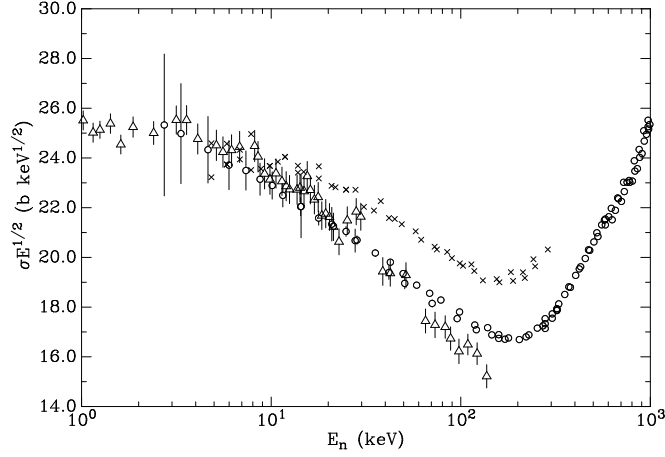


FIG. 6. The present results (\circ), compared to the data of Macklin and Gibbons [12] (\times) and the data of Borzakov *et al.* [18] (\triangle). All data are converted to ${}^3\text{He}(n,p){}^3\text{H}$ cross sections and multiplied by $E_n^{1/2}$.

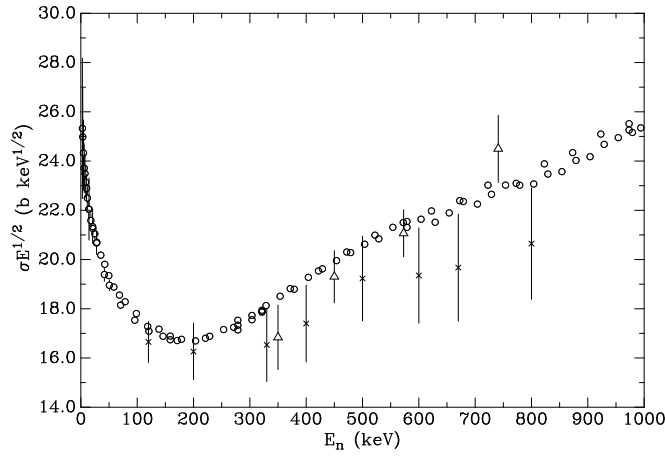


FIG. 7. The present results (\circ), compared to the data of Batchelor, Aves, and Skyrme [15] (\times) and the data of Costello, Friesenhahn, and Lopez [17] (\triangle). All data are converted to ${}^3\text{He}(n,p){}^3\text{H}$ cross sections and multiplied by $E_n^{1/2}$.

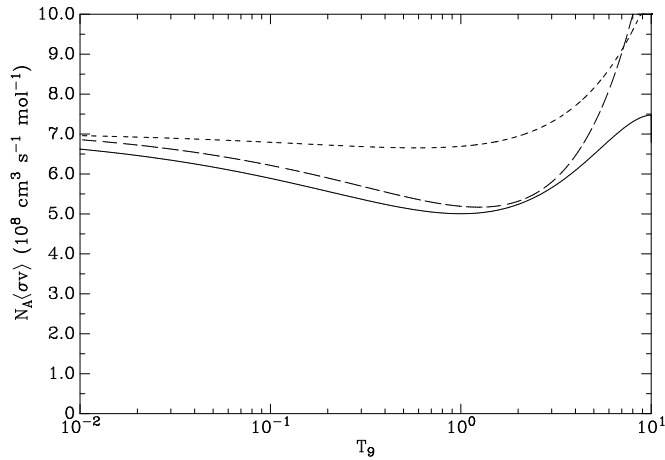


FIG. 8. The thermonuclear reaction rate $N_A\langle\sigma v\rangle$ for ${}^3\text{He}(n,p){}^3\text{H}$. The present determination is given by the solid line; the rate from Smith, Kawano, and Malaney [7] is given by the long-dashed line and the rate from Caughlan and Fowler [47] by the short-dashed line.